Evaluation of Calcium Oxide Nanoparticles from Industrial Waste on the Performance of Hardened Cement Pastes: Physicochemical Study

Authors:

Youssef Abdelatif, Abdel-Aal M. Gaber, Abd El-Aziz S. Fouda, Tarek Alsoukarry

Date Submitted: 2020-06-10

Keywords: bulk density, compressive strength, mix design, blended cement paste, calcination, calcium oxide nanoparticles

Abstract:

Large amounts of carbonated mud waste (CMW) require disposal during sugar manufacturing after the carbonation process. The lightweight of CMW enables its utilization as a partial replacement for the cement to reduce costs and CO2 emissions. Here, various levels of CMW, namely, 0, 5, 10, 15, 20, and 25 wt.% were applied to produce composite cement samples with ordinary Portland cement (OPC) as a regular mix design series. Pure calcium oxide (CaO) nanoparticles were obtained after the calcination of CMW. The techniques of X-ray fluorescence spectrometers (XRF), Transmission electron microscope (TEM), Selected area diffraction (SAED), Scanning electron microscope (SEM), energy dixpersive X-ray (EDX), and dynamic light scattering (DLS) were used to characterize the obtained CaO nanoparticles. According to the compressive strength and bulk density results, 15 wt.% CMW was optimal for the mix design. The specific surface area increased from 27.8 to 134.8 m2/g when the CMW was calcined to 600 °C. The compressive strength of the sample containing 15% CMW was lower than the values of the other pastes containing 5% and 10% CMW at all of the curing times. The porosity factor of the hardened cement pastes released with a curing time of up to 28 days. Excessive CMW of up to 25 wt.% reduced the properties of OPC.

Record Type: Published Article

Submitted To: LAPSE (Living Archive for Process Systems Engineering)

Citation (overall record, always the latest version):	LAPSE:2020.0553
Citation (this specific file, latest version):	LAPSE:2020.0553-1
Citation (this specific file, this version):	LAPSE:2020.0553-1v1

DOI of Published Version: https://doi.org/10.3390/pr8040401

processes

MDPI

Article

Evaluation of Calcium Oxide Nanoparticles from Industrial Waste on the Performance of Hardened Cement Pastes: Physicochemical Study

Youssef Abdelatif [1,2,*], Abdel-Aal M. Gaber [3], Abd El-Aziz S. Fouda [1] and Tarek Alsoukarry [4]

1 Chemistry Department, Faculty of Science, Mansoura University, Mansoura 35516, Egypt; asfouda@hotmail.com
2 Production Manager, Sugar KSA, Savola Group, Jeddah 22337, Saudi Arabia
3 Faculty of Sugar and Integrated Industries Technology and chemistry Department, Assiut University , Assiut 71516, Egypt; amabdelaal@hotmail.com
4 Raw Building Materials Technology and Processing Research Institute, Housing & Building National Research Center, HBRC, Cairo 1770, Egypt; tarek_elsokkary@yahoo.com
* Correspondence: ayoussef104@yahoo.com

Received: 27 February 2020; Accepted: 23 March 2020; Published: 30 March 2020

Abstract: Large amounts of carbonated mud waste (CMW) require disposal during sugar manufacturing after the carbonation process. The lightweight of CMW enables its utilization as a partial replacement for the cement to reduce costs and CO_2 emissions. Here, various levels of CMW, namely, 0, 5, 10, 15, 20, and 25 wt.% were applied to produce composite cement samples with ordinary Portland cement (OPC) as a regular mix design series. Pure calcium oxide (CaO) nanoparticles were obtained after the calcination of CMW. The techniques of X-ray fluorescence spectrometers (XRF), Transmission electron microscope (TEM), Selected area diffraction (SAED), Scanning electron microscope (SEM), energy dixpersive X-ray (EDX), and dynamic light scattering (DLS) were used to characterize the obtained CaO nanoparticles. According to the compressive strength and bulk density results, 15 wt.% CMW was optimal for the mix design. The specific surface area increased from 27.8 to 134.8 m^2/g when the CMW was calcined to 600 °C. The compressive strength of the sample containing 15% CMW was lower than the values of the other pastes containing 5% and 10% CMW at all of the curing times. The porosity factor of the hardened cement pastes released with a curing time of up to 28 days. Excessive CMW of up to 25 wt.% reduced the properties of OPC.

Keywords: calcium oxide nanoparticles; calcination; blended cement paste; mix design; compressive strength; bulk density

1. Introduction

Solid waste disposal in many industries is proposed for cement partial replacement, owing to the fact that these types of wastes contain some of the pozzolanic behaviour [1]. However, the improvement of the cementations characteristic of cement through partial replacement is still required. The pozzolans include different materials with high levels of silicon dioxide, which activate the hydration process [2]. Other industrial waste materials, such as blast furnace slag, fly ash, and cellulosic paper pulp, have been known to strengthen their properties [3–5]. On the other side, many studies have examined the effects of hazardous constituents such as bacteria, heavy metals, and uncontrolled organic substances [6], which have a bad effect on the ecosphere and general health. Therefore, the creation of an innovative process to maximize the recovery of beneficial materials and/or energy in a renewable way is of interest in order to protect all sides from potential threats.

In the sugar industry, sugarcane press mud is produced after the juice filtration process [7,8]. Lime milk is added into sugar juice to coagulate colloidal substances, and is settled in the form of soluble and non-soluble substances [9,10]. Subsequently, CO_2 was used as a lime surplus precipitant, and the carbonated slurry, namely carbonated mud waste (CMW), was filtered off. CMW mainly contains pure $CaCO_3$, as well as other minerals, salts, and organic compounds with coloured components [11,12]. Huge amounts of CMW disposal are generated per day during sugar manufacturing, and it is a major issue especially in eutrophication [13]. Often, CMW is used carefully or is sold as immature compost to farmers, mainly for use as a soil conditioner [14], fertilizer [15], and for wax production [16]. The richness if the micronutrient content inside the CMW enables it to be used as a fertilizer in crops and horticulture applications [17].

Ordinary Portland cement (OPC)-based concrete is the first material in construction, and the comprehensive utilization of concrete is second only to water, comprising 70% of all building and construction materials [18]. However, OPC has many advantages over geopolymers, such as the wide availability of raw materials worldwide and the ease of application, but these processes release a huge number of greenhouse gases. Statistically, one ton of cement clinker releases about 0.1 tons of CO_2, and the cement industry largely accounts for 5% of global CO_2 emissions [19].

To combat global climate change, the carbon footprint of OPC-based concrete should be reduced. To this end, the amount of OPC used in concrete needs to be reduced, as OPC is the major contributor to the carbon footprint of concrete. This can be realized by partially replacing OPC with minerals or fully replacing OPC with alternative non-OPC binders that have a lower carbon footprint [20–22]. Almost all of the published studies reported an enhancement in the mechanical properties of concrete, with up to a 10% replacement of OPC by different wastes [23–25], while a few papers also found an enhancement by splitting the tensile strength at a 15% replacement level [26,27]. Considering the literature, some authors replaced OPC with 10% and 15% bagasse ash to optimize the replacement level of OPC, but these papers did not focus on the particle size when the waste was calcined to produce ultrafine nanopowder. Nanotechnology is a trend in many applications [28–31]. Pure CaO is used in many applications, such as the cement industry, biodiesel production, the petroleum industry, electric lighting, paper industry, and power production [32–38]. There are many sources available to prepare CaO nanoparticles, such as using chicken eggshells (with very low quantities) or any source rich in calcium carbonate, such as CMW sugar cane waste, before treatment. The rheological properties of cement paste containing CaO nanoparticle contents from origin waste have not been investigated. In the present work, an attempt has been made to investigate the effect of CaO nanoparticles on the rheological behavior of the blended cement pastes. X-ray fluorescence spectrometers (XRF), Transmission electron microscope (TEM), Selected area diffraction (SAED), Scanning electron microscope (SEM), energy dixpersive X-ray (EDX), and dynamic light scattering (DLS) tools were used to analyze the properties of CaO nanoparticles. To compare the results, plain cement was also considered in the experimental program described ahead.

Herein, CMW samples were collected from different batches during the sugar production process. The physical and chemical behaviours and engineering properties were conducted in order to study the feasibility of utilizing CMW and OPC blends with various ratios. The utilization of CMW with OPC at the nanoscale seems to be a sustainable approach and may add value with many benefits, such as minimizing the burden of hauling waste to landfills and economize free spaces for disposal or to other landfills, which reduces the carbon footprint. Thereat, an environmentally and green approach would conserve precious natural aggregates and cement for future generations. On-site utilization of CMW would curtail high transportation costs, which would be highly beneficial for sites situated far from markets (high altitude regions). Finally, an aesthetic benefit includes removing waste from roadside farms.

2. Experimental Techniques

2.1. Materials, Mix Design, and Procedures

The CMW batches were collected from the Saudi Sugar Company (SGC) as semi-batches, and the samples were washed with an ethanol/double distilled water (DDI) mixture, dried, and kept in an air atmosphere to remove unfavourable odours and impurities. The samples were completely dried and crushed to reach the nominal minimum size. The specific gravity was determined to be 2.96% and the water absorption was 0.84%. The collected samples were dried at 80 °C overnight to remove the moisture content. Then, calcination at different temperatures in a muffle furnace ranging from 200 to 600 °C was applied so as to obtain nanostructured materials. In this investigation, the main hydration characteristics of the various OPC–CMW blended cement pastes consisting of mixes of M 0.0, M 0.5 CMW, M 0.10 CMW, M 0.15 CMW, M 0.20 CMW, and M 0.25 CMW were studied at various hydration time intervals of 3, 7, and 28 days. These mixes were designated as follows, based on the weight percent:

M 0.0: (100% OPC);
M 0.5: (95% OPC and 5% CMW);
M 0.10: 90% OPC and 10% CMW;
M 0.15: (85% OPC and 15% CMW);
M 0.20: (80% OPC and 20% CMW) and
M 0.25: (75% OPC and 25% CMW).

The investigated parameters were the water content of hardened cement pastes, setting times, bulk density, total porosity, and compressive strength.

2.2. Preparation of Combined Cement Pastes

A pre-determined amount of OPC was placed on a smooth, hydrophobic surface and a crater was centered. A definite amount of pure water related to cement was poured into the crater using a trowel tool. The dry OPC took for approximately five minutes in order to absorb water, and then had vigorous stirring for another five minutes in order to complete the mixing. The designed moulds had cubic dimensions of $2.5 \times 2.5 \times 2.5$ cm, and the reservoir of paste was manually pressed into the corners of moulds until a homogeneous surface was obtained. Afterwards the top layered was compacted using a thin-edged trowel to smooth the surface of the past. After moulding, the specimens were speedily cured against moisture at room temperature in a humidity reactor (100%) for at least one day. At the end of the curing period for moisturizing, the cubes were remoulded, and the curing was done hourly in tap water for 3, 7, and 28 days (ASTM: C191, 2008).

2.3. Methods of Investigation

As a preliminary measure, vicat apparatus (according to ASTM: C191, 2008) was used for determining the consistency and setting times (initial and final) of the cement pastes with water. The bulk density measurements were determined according to the following formulae:

$$\text{Bulk Density } = \frac{\text{Saturated weight}}{\text{Volume of sample}} \left(\text{g/cm}^3\right) \quad (1)$$

$$\text{The sample volume} = \frac{\text{Saturated weight} - \text{Suspended weight}}{\text{Density of water}} \left(\text{cm}^3\right) \quad (2)$$

$$\text{Bulk density} = \frac{\text{Saturated weight}}{\text{Saturated weight} - \text{Suspended weight}} \left(\text{g/cm}^3\right) \quad (3)$$

After that, the water content of the specimens and the total porosity were calculated according to the following well-known equation:

$$\text{Total porosity } (\varepsilon) = \frac{0.99W_e \times d_p}{1 + W_t} \times 100 \quad (4)$$

where 0.99 is the free water-specific volume (cm^3/g), W_e is the free water content of the paste, d_P is the paste bulk density (g/cm^3), and W_t is the saturated hardened paste of the water content.

The total porosity of the hardened cement paste is equal to the volume of the pores/the volume of the pastes. According to ASTM: C-150, 2007, the compressive strength was tested using the three cubic specimens for the same cement pastes, and the curing time was used to determine the compressive strength of the hardened paste (MPa).

2.4. Characterization

X-ray fluorescence (XRF) micro XRF analysis (Mahwah, NJ, USA) was also used to detect the included oxide after burning. Surface area measurements of nitrogen sorption/desorption were made using Brunauer–Emmett–Teller (BET) at 77 K (Gemini, GA, USA). A high-resolution transmission electron microscopy (HR-TEM) JEOL (JEM-2100, Hitachi, Japan) microscope with a high voltage of 200 kV was used. The size distribution by intensity was measured by Malvern Instruments Ltd. (Zetasizer Ver.6.32, Malvern Instruments Ltd, UK). The surface morphology was obtained by scanning electron microscopy (SEM, Sirion, MA, USA) with an acceleration voltage of 20 kV. SEM equipped with a pendent energy-dispersive X-ray spectroscopy (EDX) detector (S-3400 N II, Hitachi, Japan) was used. The thermal stability was measured by TGA thermograms in the range of 0 to 800 °C, with a constant heating rate of 5 min^{-1}.

3. Results and Discussion

3.1. Structural and Morphological Analysis of Carbonated Mud Waste (CMW) Sample

Table 2 shows the surface characteristics of the sample before and after calcination. The specific surface area (S_{BET}) before treatment was 27.8 m^2/g, then, it gradually increased to 138.8 m^2/g when subjected to a temperature of 600 °C. The pore volume was lesser in the case of the treated CMW (0.0172 cc/g), and an almost similar pore size was observed owing to the elimination of different contaminants and chemically bonded water during the formation of CaO nanoparticles [40].

Table 1. Chemical constituent of the oxide composition in the carbonated mud waste CMW using X-ray fluorescence spectrometers (XRF) analysis.

Sample (Lime Mud)	Main Constituents in (wt.%)
3.82	SiO_2
0.03	TiO_2
0.90	Al_2O_3
0.38	$Fe_2O_3{}^{tot.}$
0.61	MgO
64.73	CaO
0.22	Na_2O
0.20	K_2O
0.40	P_2O_5
0.96	SO_3
0.03	Cl
12.37	Limited oxygen index (LOI) at 550 °C

Table 1. *Cont.*

Sample (Lime Mud)	Main Constituents in (wt.%)
27.66	LOI at1000 °C
0.001	Rb_2O
0.019	MnO
0.005	NiO
0.012	CuO
0.004	ZnO
0.013	SrO

Table 1 shows the XRF of the CMW sample for recognizing the chemical content in the form of oxides after burning the sample. The chemical compositions of the CMW sample mainly contained the CaO phase formed after burning $CaCO_3$, and at a temperature of nearly 255 °C, the organic matter disappeared. Furthermore, the table lists specific contaminants associated with the process through which they are generated [33,39]. Most of the problems regarding the utilization of this sludge were attributed to the presence of these contaminants, with most of them present in soluble form. However, after treatment, most of these contaminants disappeared, which provided an opportunity for them to be blended with cement to form a paste.

Table 2. Surface behavior comparison before and after the treatment of carbonated mud waste (CMW).

Sample	Barrett, Joyner, and Halenda (BJH) Desorption Summary		
	S_{BET} (m^2/g)	Pore Volume (cc/g)	Pore Radius (nm)
CMW before	27.8	0.0982	1.983
CMW after	138.8	0.0172	1.714

Figure 1 shows the results of the HR-TEM study of CMW after calcination. Figure 1a shows a marked irregularity in both the size and shape, with a high degree of aggregation-like structures. On the other side, there are more regular structures with polygonal plate-shaped nanoparticles of five or more sides, with a mean diameter of approximately 180 nm (red cycle) [41,42]. Furthermore, the CaO nanopowder consists of roughly spherical, slightly agglomerated nanoparticles with a particle size of 90 nm (blue circles). Figure 1b reveals the pure crystal phase of the CaO nanopowder [43]. Figure 1c shows the selected area electron diffraction (SAED) patterns of the CMW nanocomposites, which confirms the successful formation of ultra-crystalline calcium nanoparticles. Figure 1d shows the SEM morphology of the calcined CMW sample. The surface texture is almost aggregated crystal grains with distinct and smooth edges connected directly with each other. In Figure 1e, as agreed before treatment and calcination, there are a lot of undesirable contaminants, as shown in EDX analysis. The treated CMW shows a strong peak was obtained at 3.69 keV because of the effect of the presence of Ca (Figure 1e inset), as revealed by EDX. The particulate amount of Ca in the final CMW was 60.67%, indicating that most of the $CaCO_3$ precursors had been converted to CaO nanoparticles. Therefore, we can conclude that the prepared CaO nanoparticles were the major component in the prepared sample.

Figure 2 shows the DLS technique for the particle size distribution analyzer for the OPC and calcined CMW. The particle size was in the range of 50–100 nm, with a narrow size distribution in the case of the CMW nanostructure; this feature of the curve indicates the suitability of the CMW fine substitution. In some cases, the grain size, particle shape, crystalline pattern, and surface chemistry can be controlled by using calcination technique through the modulation of the solution composition, solvent properties, reaction temperature, and aging time [44].

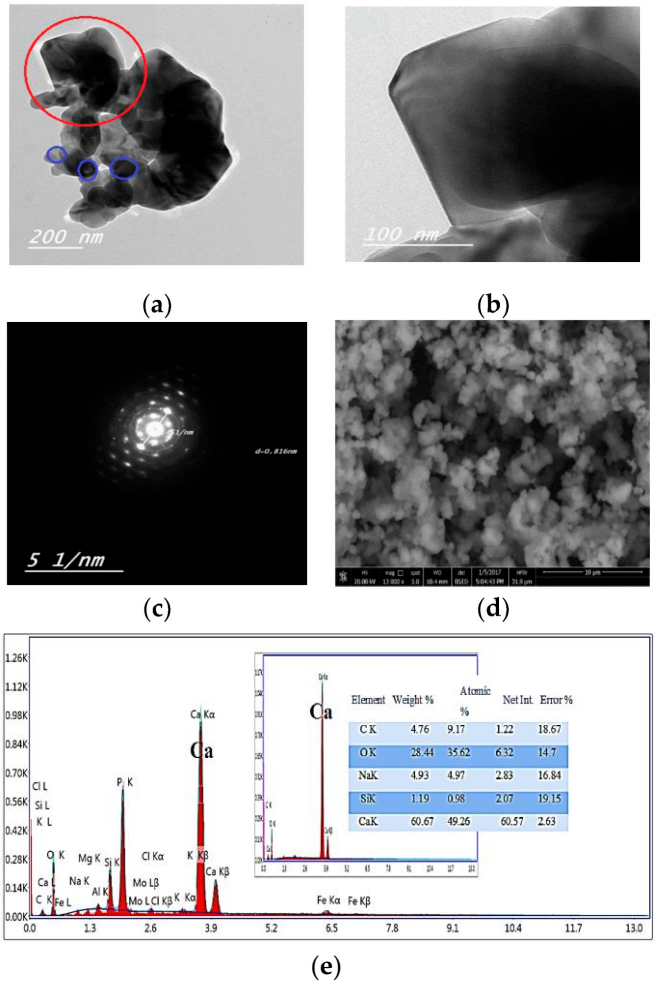

Figure 1. (**a**,**b**) TEM images of CMW with different magnification, (**c**) selected area electron diffraction (SAED) pattern for CMW, (**d**) SEM of CMW, and (**e**) EDX chart of CMW before and after calcination.

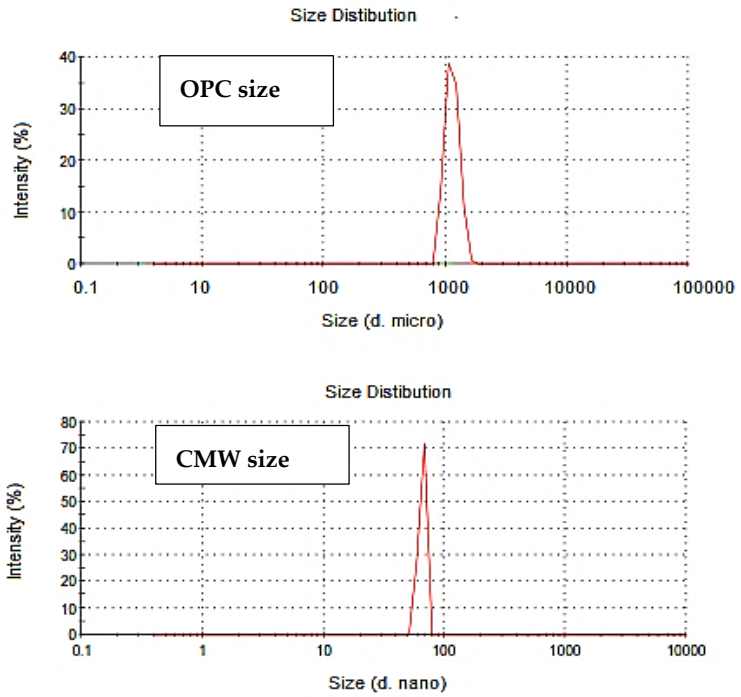

Figure 2. Particle size distribution of both cement and CMW after calcination.

3.2. Engineering Parameters

3.2.1. Compressive Strength Property

The compressive strength of OPC, including CMW, is presented in Table 3. The decrease in the hardened strength of the cement pastes containing more than 5% CMW is lower than that of the OPC at the early ages of hydration (3 days). This reinforced that the presence of the required amount of $Ca(OH)_2$ product of the hydration of OPC did not exist [45]. Also, the blended cement paste containing 15% CMW had compressive strength values lower than those of the other pastes containing 5% and 10% CMW at all of the curing ages. This result is attributed to the increase in the CMW content at the expense of OPC, which leads to the dilution of cement pastes and increased the void content, and thus resulted in decreases in compressive strength [46,47].

Table 3. Compressive strength of the ordinary Portland cement (OPC) blended cement pastes containing different ratios of calcined CMW for 3, 7, and 28 days.

Mixes	Compressive Strength (MPa)		
	3 days	7 days	28 days
OPC	52.56	69.23	71.88
OPC + 5%	34.91	61.39	69.23
OPC + 10%	31.48	53.25	67.76
OPC + 15%	30.5	47.07	51.68
OPC + 20%	30.01	42.27	47.17
OPC+ 25%	22.65	33.44	39.42

3.2.2. Bulk Density

Figure 3 shows that the bulk density nearly decreased with increasing the CMW content up to 25%, compared with the control OPC paste, which can be used as a lightweight material. In general, the results also indicate that the bulk density decreased with the increasing carbonated mud content of the OPC–CMW pastes, up to 15% (1.91 g/cm^3), in the early stage compared with the neat OPC paste (1.99 g/cm^3), owing to adding some porous calcined CMW, which had less density than the neat one [48].

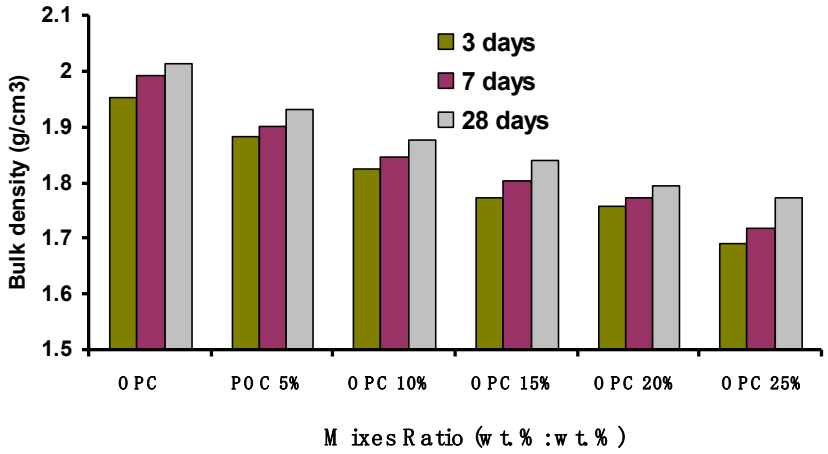

Figure 3. Bulk density of OPC and their mixes ratio with CMW.

3.2.3. Total Porosity

Figure 4 provides the total porosity of the hardened cement pastes. It has been validated that hardened cement paste is a kind of porous material [49]. The total porosity decreased with increasing the curing age to 28 days. This phenomenon is mainly because of the continuous cement hydration and

accumulation of hydration products that fill the available pores within the cement matrix, resulting in pore refinement and a reduction in the total porosity. The blended cement pastes containing 25% carbonated mud exhibited higher total porosity values at all of the curing ages than those containing 5%, 10%, 15%, and 20% carbonated mud. Increasing the carbonated mud content over the OPC led to the dilution of cement pastes and an increase in the initial porosity to a relatively high value, which is controlled by the initial water/ cement ratios (W/C), hence increasing the total porosity [50].

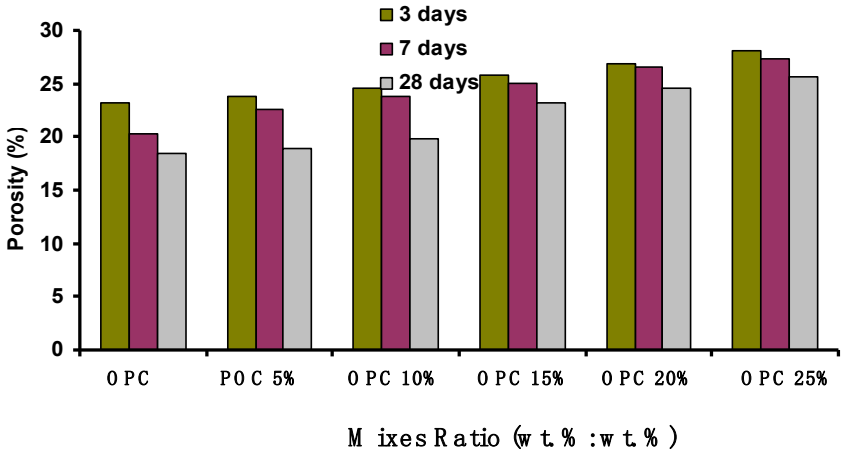

Figure 4. The total porosity of OPC and their mixes ratio with CMW.

3.2.4. Water Absorption

Water absorption was conducted to measure the amount of change in the water absorption process of CMW and the blended pastes, and the results are provided in Figure 5. The cement pastes containing carbonated mud up to 25% (20.4%) exhibited higher water absorption values at all of the curing times than the pure OPC paste. The porosity of the hardened cement paste shows that the total porosity decreased for the blended pastes, indicating that CMW-blended paste possesses a denser microstructure [51]. A high content of CMW mixed with OPC ensures the dilution of the cement paste and has a relatively high initial porosity, as controlled by the initial water/ cement ratios (W/C), hence increasing the water absorption. Furthermore, a dense microstructure is related to better anti-permeability properties, which means that blended pastes can withstand outside medium ingress, including water, so it is consistent with the water absorption test result.

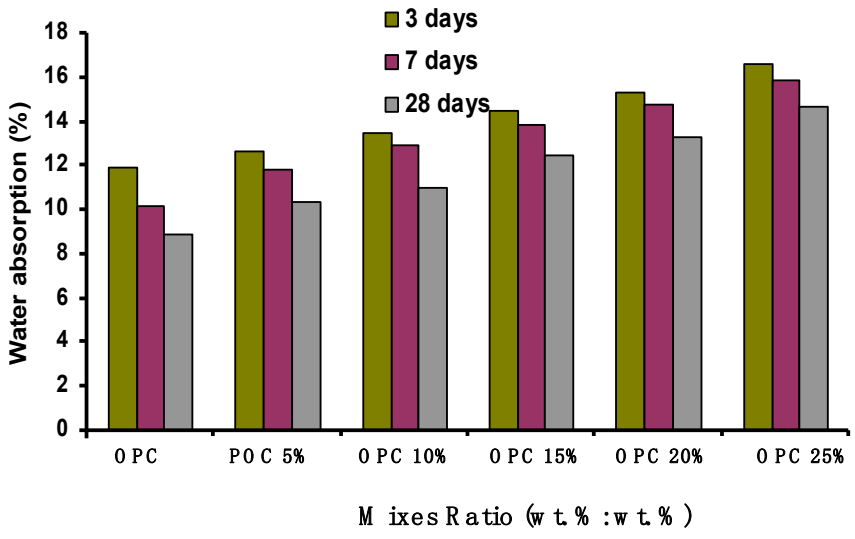

Figure 5. Water absorption of OPC and their mixes ratio with CMW.

3.2.5. Microstructure Analysis After a Fracture

Figure 6 provides the morphology of hydrated pristine OPC paste after 28 days. The SEM micrograph shows the formation of amorphous and microcrystalline phases of tobermorite-like hydrated products such as calcium silicate hydrate (CSH), along with calcium aluminate hydrates, and hexagonal calcium hydroxide; these hydrates are deposited in the originally water-filled spaces as well as in the anhydrate parts of the cement grains [52,53]. It was found that the microstructure of OPC and 5% and 10% CMW mix after 7 and 28 days of hydration formed poor crystalline particles of tobermorite-like CSH phases that were indulged, as well as the remaining anhydrate parts of cement and CMW grains. The pores that appeared in the neat OPC paste (without CMW) disappeared in this paste as a result of the filler effect of calcined CMW. The filling effect of CMW caused a notable increase in the values of compressive strength for these hardened pastes made of mixes of 5% and 10%. From the 15%, 20%, and 25% blended CM cement, partial voids could be observed, which reduced the durability.

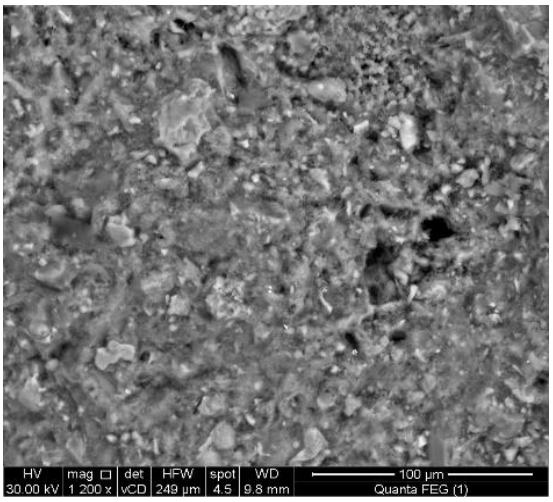

(**a**) OPC 7 days

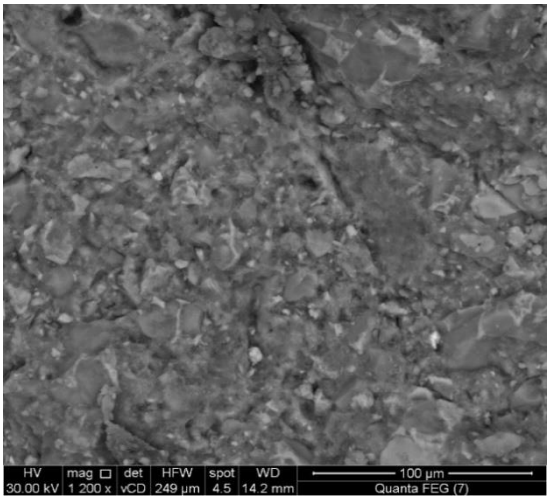

(**b**) OPC 28 days

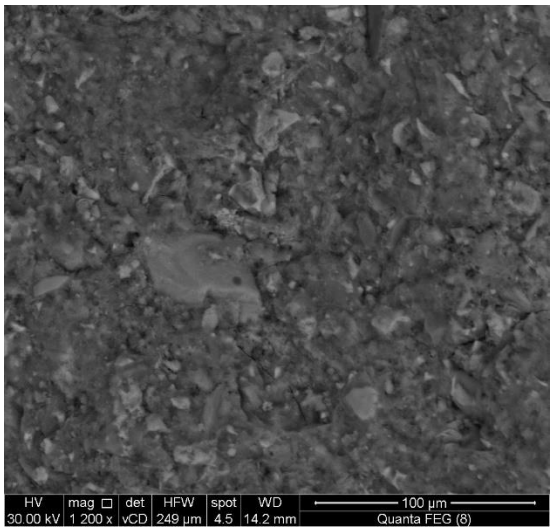

(**c**) OPC + 5% after 7 days

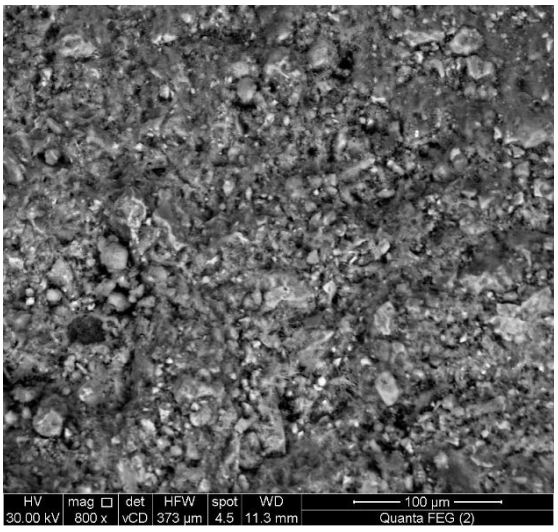

(**d**) OPC + 5% after 28 days

Figure 6. *Cont.*

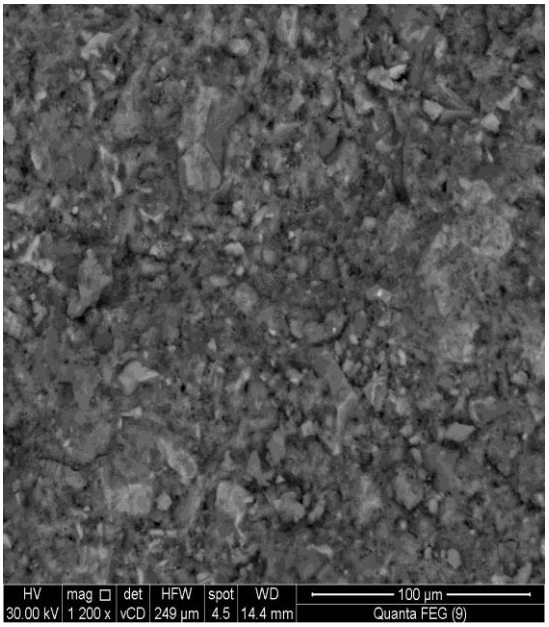

(**e**) OPC + 10% after 7 days

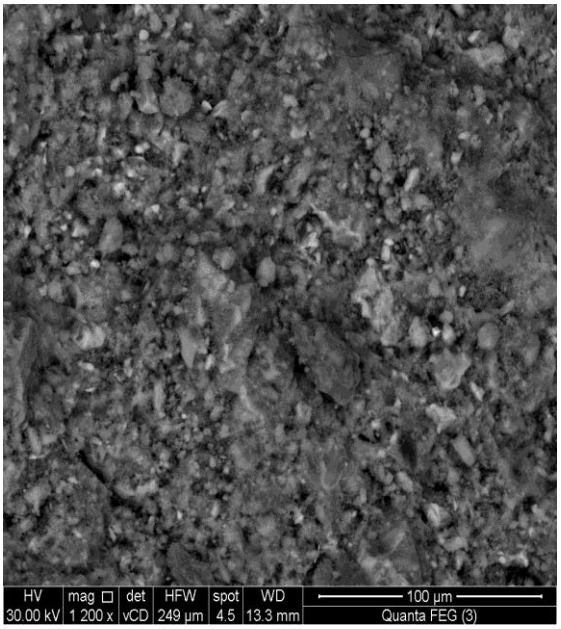

(**f**) OPC + 10% after 28 days

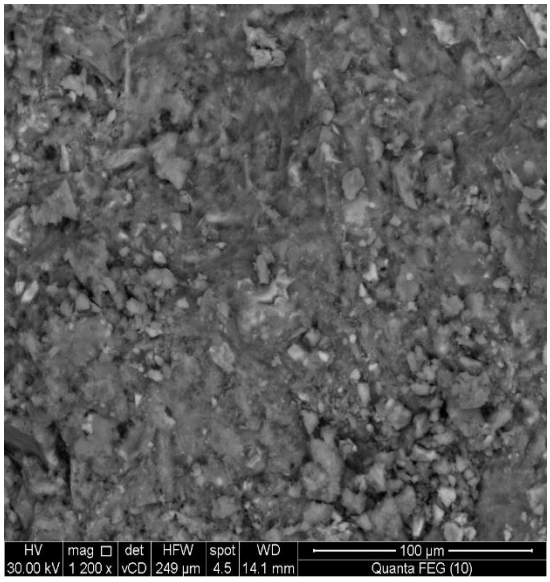

(**g**) OPC + 15% after 7 days

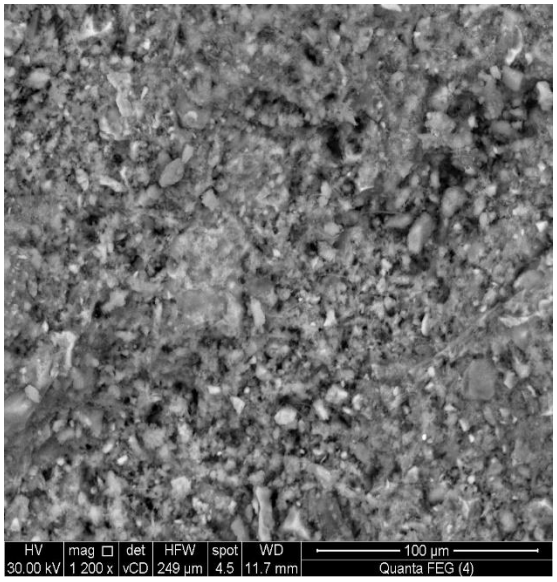

(**h**) OPC + 15% after 28 days

Figure 6. *Cont.*

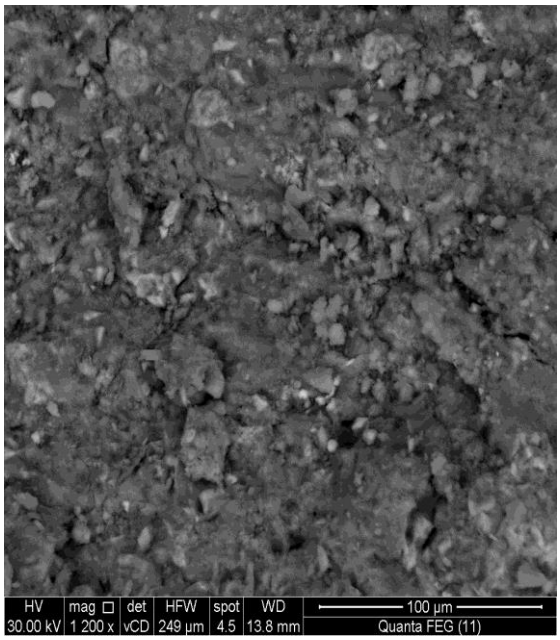

(**i**) OPC + 20% after 7 days

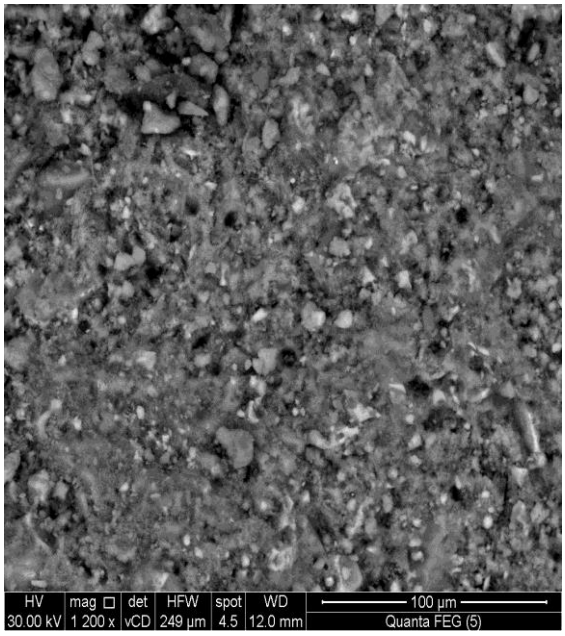

(**j**) OPC + 20% after 28 days

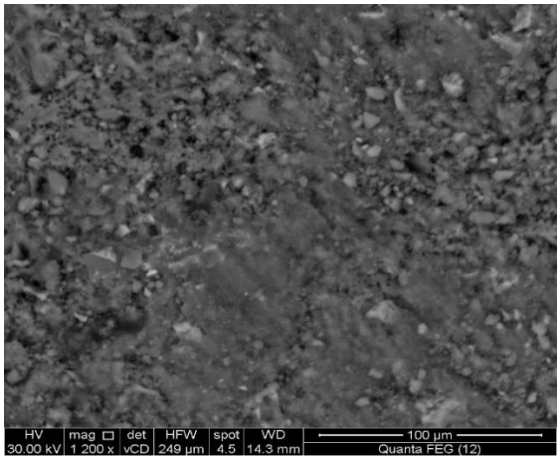

(**k**) OPC + 25% after 7 days

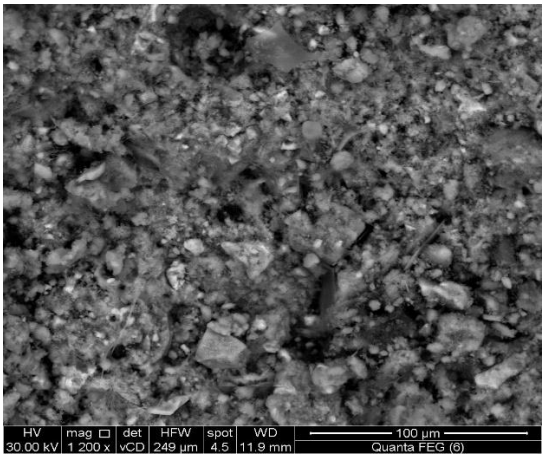

(**l**) OPC + 25% after 28 days

Figure 6. SEM micrographs of the OPC–CMW blended cement pastes at all curing times.

3.2.6. Thermal Stability Analysis

The thermal degradation stability of the mixed cement pastes containing 0%, 5%, 10%, 15%, and 20% CMW immersed in tap water for 7 days are displayed in Figure 7. The main first endothermic peak appeared at a temperature below 100 °C, because of the removal of the physically adsorbed water. The second endothermic peak was observed at approximately 100–180 °C due to the decomposition of CSH overlapping with calcium sulfoaluminate hydrates (ettringite and mono-sulfate hydrates). The third endothermic peak, located at approximately 475–500 °C, is characterized by the decomposition of portlandite $Ca(OH)_2$. The two ends of the overlapping endothermic peaks at 670–700 and 720–750 °C are related to the calcination of calcite ($CaCO_3$), with different degrees of crystallinity. The thermograms obtained for the hardened bare OPC paste display the areas and intensities of the peaks characteristic for CSH and $Ca(OH)_2$, which included the main hydration products. Beyond these areas, the peaks increase with increasing the hydration age. The effects of the partial replacement of the OPC by CMW cause a decrease in the peak area characteristic for the CSH, with increasing slag compared with that of the neat OPC paste. Furthermore, the peak area of $Ca(OH)_2$ observed in the thermograms decreased with the increasing CMW, due to the increase in their additional amounts. The thermograms obtained

for all of the hardened cement pastes show an intensive endotherm characteristic for $CaCO_3$ and an increase with an increase in the amounts of mud.

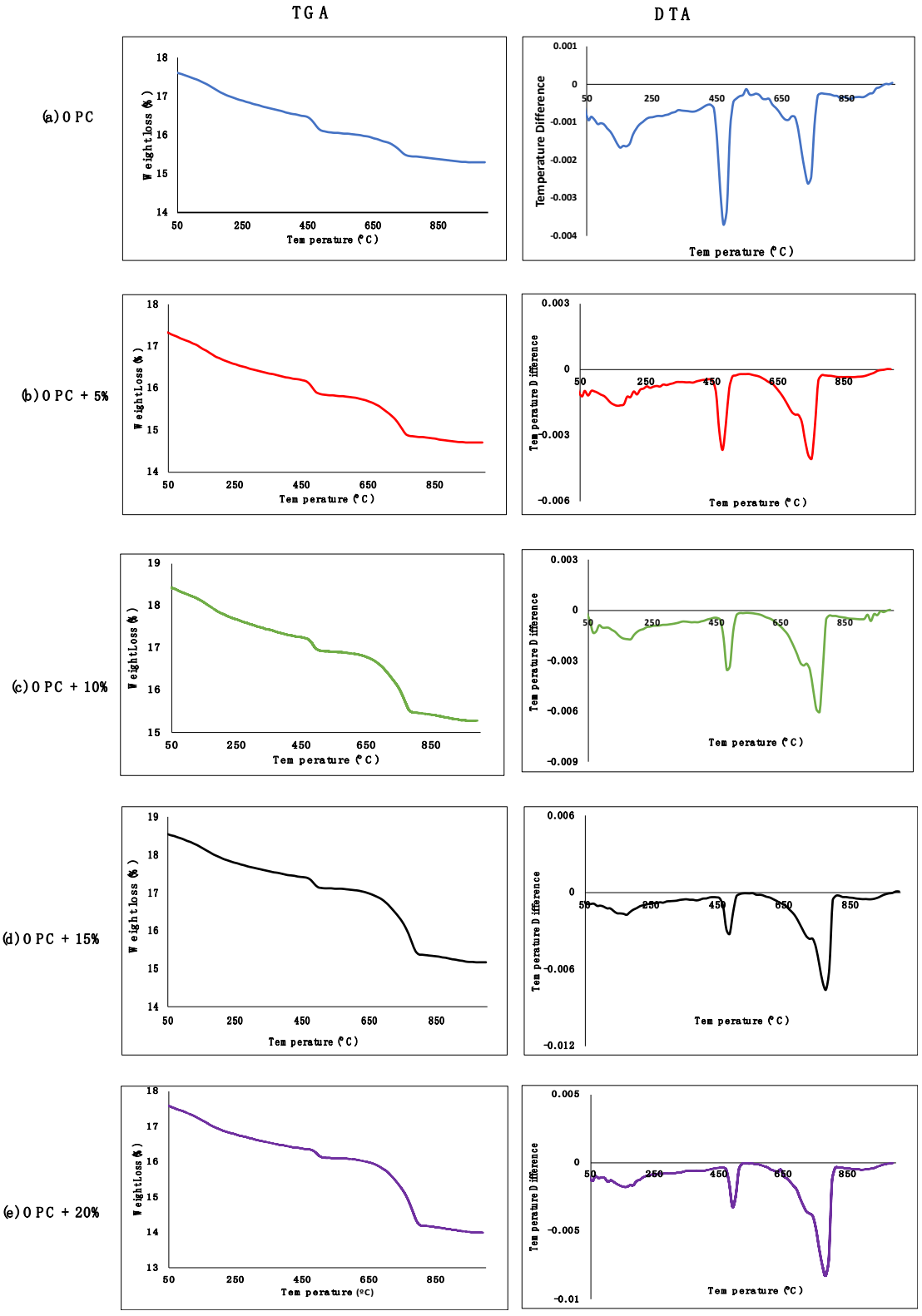

Figure 7. Thermogravimetric analysis (TGA) and differential thermal analysis (DTA) analysis of OPC–CMW blended cement pastes containing 5, 10, 15, and 20 wt. % calcined CMW nanoparticles.

3.3. Production Costs

The major goal of the present study is the argument of CMW from sugar factories, a waste originating after the carbonation process. In particular, waste materials as blended cement pastes or in the construction industry are improving the production process from economic aspects, and present an eco-friendly, viable option. Many published papers used various wastes, including palm oil mill waste [54], sewage sludge ash [55], rice husk, limestone, and the waste of activated mining coal [56]. All of the studies found that applying this disposal at a certain ratio presents a great advantage from economic, sustainable, and environmental viewpoints. Li and Yang [2] reported the utilization of Portland cement with sugar filter cake as the source of lime-based raw material, and the optimum replacement level was less than 20%. From an energy efficiency viewpoint, CMW will help reduce the need for excessive energy requirements during the stages of production, which may be beneficial for certain applications for which the energy and cost savings are vital, such as CO_2 reduction and improving the impact of climate change [57]. The incorporation of CMW not only lowered the needed energy, but also minimized the electricity consumption and saved time compared with the materials needed from natural resources. Moreover, the cost of transportation is ultimately diminished, and the economic implications of utilizing CMW instead of other costly materials, such as ZnO or TiO_2, is encouraging [58]. Mathematically, at normal operation, 60 tons of CMW are discharged per day, which requires at least six trucks. The cost of each truck is 40 SR, which is equal to $10.66. In this manner, the total annual cost equivalent was 870.000 SR ($232.222) in 2018, for example. Therefore, incorporating CMW into OPC enhances the cost-saving criteria and inserts green building infrastructure components to improve the engineering economy factor.

4. Conclusions

In summary, important considerations and informative data were presented to evaluate the feasibility of utilizing calcined CMW (5–25 wt. %) from a sugar refining company in the cement industry. The expected outcomes from this study provide guidelines regarding the characteristics of CMW, its engineering performance, and its sustainability. According to the overall methodology and characterization tests, the variation in the results for the different samples is not substantial, but a level of 15 wt.% is nearly acceptable and suitable for all of the parameters of hardened cement paste, as it contributes to a better waste management system, improves the sustainability in the cement industry, and prevents pathogenic effects during transportation. The small particle size of CaO with an average of ~50–100 nm is satisfactory for OPC compatibility. The compressive strength values (kg/cm^2) were studied for all of the curing ages. The engineering and environmental impacts were also affirmative concerning the amount of greenhouse gas emissions, daily energy consumption, and economic factors. Furthermore, CMW can reduce the cost of construction by up to $230 per year.

Author Contributions: Conceptualization, Y.A.; Data curation, A.-A.M.G. and A.E.-A.S.F.; Investigation, T.A. All authors have read and agreed to the published version of the manuscript.

Funding: This research received no external funding.

Conflicts of Interest: The authors declare no conflict of interest.

References

1. Saeli, M.; Tobaldi, D.M.; Seabra, M.P.; Labrincha, J.A. Mix design and mechanical performance of geopolymeric binders and mortars using biomass fly ash and alkaline effluent from paper-pulp industry. *J. Clean. Prod.* **2019**, *208*, 1188–1197. [CrossRef]
2. Li, H.; Xu, W.; Yang, X.; Wu, J. Preparation of Portland cement with sugar filter mud as lime-based raw material. *J. Clean. Prod.* **2014**, *66*, 107–112. [CrossRef]
3. Huang, H.; Ye, G.; Damidot, D. Effect of blast furnace slag on self-healing of microcracks in cementitious materials. *Cem. Concr. Res.* **2014**, *60*, 68–82. [CrossRef]
4. Naidu, P.V.; Pandey, P.K. Replacement of cement in concrete. *Int. J. Environ. Res. Dev.* **2014**, *4*, 91–98.

5. Balwaik, S.A.; Raut, S. Utilization of waste paper pulp by partial replacement of cement in concrete. *Int. J. Eng. Res. Appl.* **2011**, *1*, 300–309.
6. Reddy, K.R.; Gopakumar, A.; Chetri, J.K. Critical review of applications of iron and steel slags for carbon sequestration and environmental remediation. *Rev. Environ. Sci. Bio/Technol.* **2019**, *18*, 127–152. [CrossRef]
7. Payá, J.; Monzó, J.; Borrachero, M.V.; Díaz-Pinzón, L.; Ordonez, L.M. Sugar-cane bagasse ash (SCBA): Studies on its properties for reusing in concrete production. *J. Chem. Technol. Biotechnol. Int. Res. Process Environ. Clean Technol.* **2002**, *77*, 321–325. [CrossRef]
8. Arif, E.; Clark, M.W.; Lake, N. Sugar cane bagasse ash from a high efficiency co-generation boiler: Applications in cement and mortar production. *Constr. Build. Mater.* **2016**, *128*, 287–297. [CrossRef]
9. Fairbairn, E.M.; Americano, B.B.; Cordeiro, G.C.; Paula, T.P.; Filho, R.D.T.; Silvoso, M.M. Cement replacement by sugar cane bagasse ash: CO2 emissions reduction and potential for carbon credits. *J. Environ. Manag.* **2010**, *91*, 1864–1871. [CrossRef]
10. Atta, A.M.; Abdel-Bary, E.; Rezk, K.; Abdel-Azim, A. Fast responsive poly (acrylic acid-co-N-isopropyl acrylamide) hydrogels based on new crosslinker. *J. Appl. Polym. Sci.* **2009**, *112*, 114–122. [CrossRef]
11. Sua-Iam, G.; Makul, N. Use of increasing amounts of bagasse ash waste to produce self-compacting concrete by adding limestone powder waste. *J. Clean. Prod.* **2013**, *57*, 308–319. [CrossRef]
12. El-Shabasy, R.; Yosri, N.; El-Seedi, H.; Shoueir, K.; El-Kemary, M. A green synthetic approach using chili plant supported Ag/Ag2O@ P25 heterostructure with enhanced photocatalytic properties under solar irradiation. *Optik* **2019**, *192*, 162943. [CrossRef]
13. Li, H.; Xu, J.; Wu, J.; Xu, W.; Xu, Y. Influence of sugar filter mud on formation of portland cement clinker. *J. Wuhan Univ. Technol. Mater. Sci. Ed.* **2013**, *28*, 746–750. [CrossRef]
14. Madejón, E.; López, R.; Murillo, J.M.; Cabrera, F. Agricultural use of three (sugar-beet) vinasse composts: Effect on crops and chemical properties of a Cambisol soil in the Guadalquivir river valley (SW Spain). *Agric. Ecosyst. Environ.* **2001**, *84*, 55–65. [CrossRef]
15. Anacleto, L.R.; Roberto, M.M.; Marin-Morales, M.A. Toxicological effects of the waste of the sugarcane industry, used as agricultural fertilizer, on the test system Allium cepa. *Chemosphere* **2017**, *173*, 31–42. [CrossRef] [PubMed]
16. Burman, N.W.; Harding, K.G.; Sheridan, C.M.; van Dyk, L. Evaluation of a combined lignocellulosic/waste water bio-refinery for the simultaneous production of valuable biochemical products and the remediation of acid mine drainage. *Biofuels Bioprod. Biorefin.* **2018**, *12*, 649–664. [CrossRef]
17. Kapur, M.; Kanwar, R. Influence of cane filter cakes and cattle manure on micronutrients content in sugar-beet and their availability in alkaline sandy loam soil. *Biol. Wastes* **1989**, *29*, 233–238. [CrossRef]
18. Xu, Q.; Ji, T.; Gao, S.-J.; Yang, Z.; Wu, N. Characteristics and Applications of Sugar Cane Bagasse Ash Waste in Cementitious Materials. *Materials* **2019**, *12*, 39. [CrossRef]
19. Paris, J.M.; Roessler, J.G.; Ferraro, C.C.; DeFord, H.D.; Townsend, T.G. A review of waste products utilized as supplements to Portland cement in concrete. *J. Clean. Prod.* **2016**, *121*, 1–18. [CrossRef]
20. Moretti, J.P.; Sales, A.; Almeida, F.C.; Rezende, M.A.; Gromboni, P.P. Joint use of construction waste (CW) and sugarcane bagasse ash sand (SBAS) in concrete. *Constr. Build. Mater.* **2016**, *113*, 317–323. [CrossRef]
21. Gopinath, A.; Bahurudeen, A.; Appari, S.; Nanthagopalan, P. A circular framework for the valorisation of sugar industry wastes: Review on the industrial symbiosis between sugar, construction and energy industries. *J. Clean. Prod.* **2018**, *203*, 89–108. [CrossRef]
22. Singh, S.; Ransinchung, G.; Debbarma, S.; Kumar, P. Utilization of reclaimed asphalt pavement aggregates containing waste from Sugarcane Mill for production of concrete mixes. *J. Clean. Prod.* **2018**, *174*, 42–52. [CrossRef]
23. Singh, S.; Ransinchung, G.; Kumar, P. An economical processing technique to improve RAP inclusive concrete properties. *Constr. Build. Mater.* **2017**, *148*, 734–747. [CrossRef]
24. Bahurudeen, A.; Kanraj, D.; Dev, V.G.; Santhanam, M. Performance evaluation of sugarcane bagasse ash blended cement in concrete. *Cem. Concr. Compos.* **2015**, *59*, 77–88. [CrossRef]
25. Gar, P.S.; Suresh, N.; Bindiganavile, V. Sugar cane bagasse ash as a pozzolanic admixture in concrete for resistance to sustained elevated temperatures. *Constr. Build. Mater.* **2017**, *153*, 929–936.
26. Modani, P.O.; Vyawahare, M. Utilization of bagasse ash as a partial replacement of fine aggregate in concrete. *Procedia Eng.* **2013**, *51*, 25–29. [CrossRef]

27. Loh, Y.; Sujan, D.; Rahman, M.E.; Das, C.A. Sugarcane bagasse—The future composite material: A literature review. *Resour. Conserv. Recycl.* **2013**, *75*, 14–22. [CrossRef]
28. Shaban, N.Z.; Yehia, S.A.; Shoueir, K.R.; Saleh, S.R.; Awad, D.; Shaban, S.Y. Design, DNA binding and kinetic studies, antibacterial and cytotoxic activities of stable dithiophenolato titanium (IV)-chitosan Nanocomposite. *J. Mol. Liq.* **2019**, *287*, 111002. [CrossRef]
29. Shoueir, K.; Ahmed, M.; Gaber, S.A.A.; El-Kemary, M. Thallium and selenite doped carbonated hydroxyapatite: Microstructural features and anticancer activity assessment against human lung carcinoma. *Ceram. Int.* **2020**, *46*, 5201–5212. [CrossRef]
30. Abdelbar, M.F.; El-Sheshtawy, H.S.; Shoueir, K.R.; El-Mehasseb, I.; Ebeid, E.-Z.M.; El-Kemary, M. Halogen bond triggered aggregation induced emission in an iodinated cyanine dye for ultra sensitive detection of Ag nanoparticles in tap water and agricultural wastewater. *RSC Adv.* **2018**, *8*, 24617–24626. [CrossRef]
31. Salama, A.; Diab, M.A.; Abou-Zeid, R.E.; Aljohani, H.A.; Shoueir, K.R. Crosslinked alginate/silica/zinc oxide nanocomposite: A sustainable material with antibacterial properties. *Compos. Commun.* **2018**, *7*, 7–11. [CrossRef]
32. Oualha, M.A.; Omri, N.; Oualha, R.; Nouioui, M.A.; Abderrabba, M.; Amdouni, N.; Laoutid, F. Development of metal hydroxide nanoparticles from eggshell waste and seawater and their application as flame retardants for ethylene-vinyl acetate copolymer (EVA). *Int. J. Biol. Macromol.* **2019**, *128*, 994–1001. [CrossRef] [PubMed]
33. El-Kemary, M.A.; El-mehasseb, I.M.; Shoueir, K.R.; El-Shafey, S.E.; El-Shafey, O.I.; Aljohani, H.A.; Fouad, R.R. Sol-gel TiO_2 decorated on eggshell nanocrystal as engineered adsorbents for removal of acid dye. *J. Dispers. Sci. Technol.* **2018**, *39*, 911–921. [CrossRef]
34. Naveenkumar, R.; Baskar, G. Biodiesel production from Calophyllum inophyllum oil using Zinc doped Calcium oxide (Plaster of Paris) nanocatalyst. *Bioresour. Technol.* **2019**, *280*, 493–496. [CrossRef] [PubMed]
35. Benzennou, S.; Laviolette, J.P.; Chaouki, J. Kinetic study of microwave pyrolysis of paper cups and comparison with calcium oxide catalyzed reaction. *AIChE J.* **2018**, *65*, 684–690. [CrossRef]
36. Jiménez, P.E.S.; Perejón, A.; Guerrero, M.B.; Valverde, J.M.; Ortiz, C.; Maqueda, L.A.P. High-performance and low-cost macroporous calcium oxide based materials for thermochemical energy storage in concentrated solar power plants. *Appl. Energy* **2019**, *235*, 543–552. [CrossRef]
37. Rieger, J.; Kellermeier, M.; Nicoleau, L. Formation of nanoparticles and nanostructures—An industrial perspective on $CaCO_3$, cement, and polymers. *Angew. Chem. Int. Ed.* **2014**, *53*, 12380–12396. [CrossRef]
38. Atta, A.M.; El-Mahdy, G.A.; Al-Lohedan, H.A.; Shoueir, K.R. Electrochemical behavior of smart N-isopropyl acrylamide copolymer nanogel on steel for corrosion protection in acidic solution. *Int. J. Electrochem. Sci.* **2015**, *10*, 870–882.
39. Gunning, P.J.; Hills, C.D.; Carey, P.J. Accelerated carbonation treatment of industrial wastes. *Waste Manag.* **2010**, *30*, 1081–1090. [CrossRef]
40. Kočí, K.; Matějka, V.; Kovář, P.; Lacný, Z.; Obalová, L. Comparison of the pure TiO_2 and kaolinite/TiO_2 composite as catalyst for CO_2 photocatalytic reduction. *Catal. Today* **2011**, *161*, 105–109. [CrossRef]
41. Shoueir, K.; El-Sheshtawy, H.; Misbah, M.; El-Hosainy, H.; El-Mehasseb, I.; El-Kemary, M. Fenton-like nanocatalyst for photodegradation of methylene blue under visible light activated by hybrid green DNSA@ Chitosan@ $MnFe_2O_4$. *Carbohydr. Polym.* **2018**, *197*, 17–28. [CrossRef] [PubMed]
42. Shoueir, K.; Kandil, S.; El-hosainy, H.; El-Kemary, M. Tailoring the surface reactivity of plasmonic Au@ TiO_2 photocatalyst bio-based chitosan fiber towards cleaner of harmful water pollutants under visible-light irradiation. *J. Clean. Prod.* **2019**, *230*, 383–393. [CrossRef]
43. Abdel-Gawwad, H.; Heikal, M.; Mohammed, M.S.; El-Aleem, S.A.; Hassan, H.S.; García, S.V.; Rashad, A.M. Evaluating the impact of nano-magnesium calcite waste on the performance of cement mortar in normal and sulfate-rich media. *Constr. Build. Mater.* **2019**, *203*, 392–400. [CrossRef]
44. Habte, L.; Shiferaw, N.; Mulatu, D.; Thenepalli, T.; Chilakala, R.; Ahn, J.W. Synthesis of Nano-Calcium Oxide from Waste Eggshell by Sol-Gel Method. *Sustainability* **2019**, *11*, 3196. [CrossRef]
45. Rashad, A.M. An exploratory study on high-volume fly ash concrete incorporating silica fume subjected to thermal loads. *J. Clean. Prod.* **2015**, *87*, 735–744. [CrossRef]
46. Nguyen, H.-A.; Chang, T.-P.; Shih, J.-Y.; Chen, C.-T. Influence of low calcium fly ash on compressive strength and hydration product of low energy super sulfated cement paste. *Cem. Concr. Compos.* **2019**, *99*, 40–48. [CrossRef]

47. Fouad, R.R.; Aljohani, H.A.; Shoueir, K.R. Biocompatible poly (vinyl alcohol) nanoparticle-based binary blends for oil spill control. *Mar. Pollut. Bull.* **2016**, *112*, 46–52. [CrossRef]
48. Kroehong, W.; Jaturapitakkul, C.; Pothisiri, T.; Chindaprasirt, P. Effect of Oil Palm Fiber Content on the Physical and Mechanical Properties and Microstructure of High-Calcium Fly Ash Geopolymer Paste. *Arab. J. Sci. Eng.* **2018**, *43*, 5215–5224. [CrossRef]
49. Seleem, H.E.D.H.; Rashad, A.M.; Elsokary, T. Effect of elevated temperature on physico-mechanical properties of blended cement concrete. *Constr. Build. Mater.* **2011**, *25*, 1009–1017. [CrossRef]
50. Seleem, H.E.-D.H.; Rashad, A.M.; Elsokary, T. The Impact of Pozzolana in Securing Fire-resistive Properties of Concrete. *Silic. Ind.* **2009**, *9*, 245–254.
51. Wang, W.; Liu, X.; Guo, L.; Duan, P. Evaluation of Properties and Microstructure of Cement Paste Blended with Metakaolin Subjected to High Temperatures. *Materials* **2019**, *12*, 941. [CrossRef] [PubMed]
52. Amin, M.; El-Gamal, S.; Abo-El-Enein, S.; El-Hosiny, F.; Ramadan, M. Physico-chemical characteristics of blended cement pastes containing electric arc furnace slag with and without silica fume. *HBRC J.* **2015**, *11*, 321–327. [CrossRef]
53. Polat, R.; Demirboğa, R.; Karagöl, F. Mechanical and physical behavior of cement paste and mortar incorporating nano-CaO. *Struct. Concr.* **2019**, *20*, 361–370. [CrossRef]
54. Kanadasan, J.; Fauzi, A.; Razak, H.; Selliah, P.; Subramaniam, V.; Yusoff, S. Feasibility studies of palm oil mill waste aggregates for the construction industry. *Materials* **2015**, *8*, 6508–6530. [CrossRef] [PubMed]
55. Baeza-Brotons, F.; Garcés, P.; Payá, J.; Saval, J.M. Portland cement systems with addition of sewage sludge ash. Application in concretes for the manufacture of blocks. *J. Clean. Prod.* **2014**, *82*, 112–124. [CrossRef]
56. Mejia-Ballesteros, J.E.; Savastano, H., Jr.; Fiorelli, J.; Rojas, M.F. Effect of mineral additions on the microstructure and properties of blended cement matrices for fibre-cement applications. *Cem. Concr. Compos.* **2019**, *98*, 49–60. [CrossRef]
57. Gartner, E.; Hirao, H. A review of alternative approaches to the reduction of CO_2 emissions associated with the manufacture of the binder phase in concrete. *Cem. Concr. Res.* **2015**, *78*, 126–142. [CrossRef]
58. Senff, L.; Tobaldi, D.; Lemes-Rachadel, P.; Labrincha, J.; Hotza, D. The influence of TiO_2 and ZnO powder mixtures on photocatalytic activity and rheological behavior of cement pastes. *Constr. Build. Mater.* **2014**, *65*, 191–200. [CrossRef]